Weakening of the Atlantic Meridional Overturning Circulation Abyssal Limb in the North Atlantic

Tiago Carrilho Biló[1,2*], Renellys C. Perez[2], Shenfu Dong[2],
William Johns[3], and Torsten Kanzow[4,5]

[1]Cooperative Institute for Marine and Atmospheric Studies, University of Miami, 4600 Rickenbacker Causeway, Miami, FL 33149, United States

[2]Atlantic Oceanographic and Meteorological Laboratory, National Oceanic and Atmospheric Administration, 4301 Rickenbacker Causeway, Miami, FL 33149, United States

[3]Rosenstiel School of Marine, Atmospheric, and Earth Science, University of Miami, 4600 Rickenbacker Causeway, Miami, FL 33149, United States

[4]Climate Sciences Division, Alfred-Wegener-Institute Helmholtz Center for Polar and Marine Research, Am Handelshafen 12, Bremerhaven, 27570, Germany

[5]Department of Physics and Electrical Engineering, University of Bremen, Otto-Hahn-Allee 1, Bremen, 28359, Germany

*Corresponding author e-mail: tiago.bilo@noaa.gov

Contributing author e-mails: renellys.c.perez@noaa.gov; shenfu.dong@noaa.gov; bjohns@rsmas.miami.edu; torsten.kanzow@awi.de;

for publication in

Nature Geoscience

Abstract

The abyssal limb of the global Meridional Overturning Circulation redistributes heat and carbon as it carries Antarctic Bottom Water from the Southern Ocean towards the northern hemisphere. Using mooring observations and hydrographic data from multiple sources in the North Atlantic, we show that northward flowing Antarctic Bottom Water is constrained below 4500 m with a mean volume transport of 2.40 ±0.2 5 Sv at 16°N. We find that during 2000-2020, the Antarctic Bottom Water northward transport weakened by approximately 0.35 ± 0.13 Sv, corresponding to a 12 ± 5% decrease. The weakening of the Atlantic Meridional Overturning Circulation abyssal cell is a probable response to reduced Antarctic Bottom Water formation rates over the past several decades and is associated with abyssal warming observed throughout the Western Atlantic Ocean. We estimate that the warming of the Antarctic Bottom Water layer in the subtropical North Atlantic is, on average, 1 m°C/year in the last two decades due to the downward heaving of abyssal isopycnals, contributing to the increase of abyssal heat content and, hence, sea-level rise in the region. This warming trend is approximately half of the Antarctic Bottom Water warming trend observed in the South Atlantic and parts of the Southern Ocean, indicating a dilution of the signal as the Antarctic Bottom Water crosses the Equator.

Key words: AMOC weakening, Antarctic Bottom Water, deep ocean circulation, abyssal warming

Introduction

The Antarctic Bottom Water (AABW) forms through a myriad of physical processes along the Antarctic continent, comprising the world's oceans' coldest and densest water masses [1]. As it spreads northward, it redistributes large amounts of heat and carbon within the deepest limb of the global Meridional Overturning Circulation (MOC) [2], filling most of the ocean's deep (1000< depth< 4000 m) and abyssal (depth >4000 m) areas [3]. Therefore, significant water temperature and circulation variations within this cold but vast water reservoir have a global impact on Earth's heat budget [4, 5] and sea level rise [6, 7].

The AABW has significantly warmed since the 1980s around the globe, with the observed warming rates up to 5 m°C $year^{-1}$ near the AABW's formation sites [6, 8-15]. In certain regions like the Australian Antarctic Basin, there is evidence of AABW warming and freshening started much earlier since the 1960s [16]. Analysis of repeated hydrography surveys suggests that this

warming is associated with the downward displacement of isopycnals, indicating a potential decrease of the AABW's total volume in the abyssal oceans consistent with the reduction in AABW's formation rates in the past five decades [17].

Both data assimilation [7, 18] and non-assimilative numerical experiments [19, 20] suggest that a decrease in the AABW formation rates and, consequently, a slow-down of the northward AABW flow could trigger a series of Kelvin and Rossby waves that can bring such anomalies to northern areas of the oceanic basins on decadal time scales [18, 19] instead of the expected advective travel times of hundreds to thousands of years [21]. Specifically in the Atlantic Ocean, where the primary AABW source is the Weddell Sea [22, 23], [20] showed that this simulated fast oceanic response to changes around the Southern Ocean is not only associated with the possible weakening and warming of the northward abyssal limb of the Atlantic MOC (AMOC) but also with the acceleration of the flow within the deep and upper layers of the AMOC. Although the northward progression of the warming signal could be partially explained by the advection of the slow abyssal flow, [20] verified that the onset of the quasi-linear warming trends in the Vema Channel at 30°S (also present in observations since the late 1970s [24]) and northward is likely explained by the wave response. While this dynamic ocean adjustment process is a robust feature of different types of numerical simulations, suggesting the ongoing climate change will continue to induce the global abyssal ocean to warm for the foreseeable future[25], observational studies of the abyssal North Atlantic have reported vigorous variability showing no evidence of statistically robust long-term trends after 2000 [26, 27].

The AABW enters the North Atlantic Basin primarily between the South American continent and the Mid-Atlantic Ridge (MAR) below the North Atlantic Deep Water (NADW) and reaches as far poleward as 40°N (see 1.8°C isotherm, or AABW and NADW interface, in Fig. 1a). While part of this abyssal flow could penetrate the basin's eastern side through large fracture zones along the MAR, the bulk of AABW continues to spread to the west of the MAR [9, 28-30]. North of 16°N, measurements from multiple repeated hydrographic transects in the western North Atlantic obtained between 1981-2004 indicated that the AABW volume reduced by up to 30-40% during this period [9], suggesting a possible halt of the AABW inflow to the North Atlantic Ocean in the coming decades.

Although abyssal geostrophic transport estimates at 24.5°N from repeated hydrographic surveys corroborated [9]'s results, the same dataset extended between 1957-2010 plus six months of moored records showed that the AABW geostrophic transports exhibit variability from daily to interannual time scales [26], making it difficult to ascertain any longer-term AABW transport trends, especially after 1998. Additionally, these repeated surveys up to 2004 revealed that cooling along isopycnal surfaces associated with abyssal freshening surpassed the abyssal warming signal driven by the contraction of the AABW cold layer [31]. Finally, recent temperature analyses of the entire abyssal western North Atlantic between 4000-6000 m indicated that these areas slightly cooled between 2000-2014 due to both abyssal freshening and vertical expansion of the abyssal layers [27], opposing the observed North Atlantic's 1980s-2000 and South Atlantic's 1970s-present warming tendencies [6, 9, 10, 15, 24, 26, 32]. Although some of the cited hydrographic changes associated with small salinity variations observed before 2000 should be interpreted with caution due to larger uncertainties [33], the vigorous abyssal temperature and transport variability at different time scales reported by multiple studies put into question the persistence of the slow-down of the abyssal AMOC and its associated warming in the North Atlantic basin in the 21st century.

In the present study, we use moored hydrographic observations, multiple hydrographic cruise surveys, and Deep Argo profiles (Fig. 1a) to quantify the variability of the AABW inflow to the subtropical North Atlantic on interannual-to-longer time scales and the associated abyssal warming trends in the first two decades of the 21st century. We found robust observational evidence for a persistent kinematic weakening of the AMOC's abyssal limb in the North Atlantic Ocean between 2000-2020, suggesting that the AABW formation and volume reduction signal in the Southern Hemisphere continuously penetrated the region during that period, increasing the abyssal heat content and contributing to the sea-level rise.

Weakening of the North Atlantic Abyssal Circulation

Across 16°N, the northward flowing AABW layer is mainly limited to below 4500 m (Fig. 1b). Most of the AABW seems to be flowing northward within the abyssal current above the western flank of the MAR with maximum velocities of about 3-4×10^{-2} m s^{-1} below 5000 m (Fig. 1c), in agreement with observations [26, 31, 34-36] and idealized simulations [37] of the abyssal flow in the Atlantic Ocean. Not surprisingly, geostrophic velocity profiles relative to

4500 m averaged across this area reveal that the northward flow increases with depth below 4500 m, peaks between 5000-5200 m, and then decreases to approximately zero between ~5500-5800 m (Fig. 2a). Integrating the abyssal geostrophic velocity along 16°N and below 4500 m, we find a mean AABW transport of 2.40 ± 0.25 Sv. The hydrographic mooring observations also indicate that the AABW transport is weakening at a rate of $1.75 \pm 0.65 \times 10^{-2}$ Sv year^{-1} since 2000 (Fig. 2b). Over approximately 20 years, the AABW transport reduced by 0.35 ± 0.13 Sv, corresponding to $12 \pm 5\%$ of the annual mean transport in 2000. Besides the significant long-term trend, the abyssal transports exhibit substantial interannual variability. The most prominent events are the strong decrease in 2008-2010 of 0.65 Sv and the 0.50 Sv transport recovery in 2016-2017.

Because we referenced our mooring-based geostrophic transport estimates to a constant depth (see methods), their variability mainly arises from changes in the vertical geostrophic shear, which are proportional to horizontal density gradient variations across 16°N. The observed 20-year-long AABW transport reduction (Fig. 2b) resulted from the decrease of the geostrophic shear below ~4600 m (Fig. 3a). Since the isotherms and isopycnals within the AABW layer tend to rise eastward (Figs. 1b-1c), a warming/freshening of AABW near the western flank of the MAR would act to flatten the isopycnals and, consequently, weaken the abyssal geostrophic flow. We find that the abyssal warming near the MAR is the primary contributor to the isopycnal flattening associated with the long-term weakening of the AABW transport.

While the vertical shear (Fig. 3c, solid green line) is decreasing at a rate approximately the same as the shear due to the warming near the MAR (i.e., $\sim -3.8 \pm 1 \times 10^{-8}$ s^{-1} year^{-1}) (Fig. 3c, dashed magenta line), the density changes within the DWBC (i.e., NADW flow) impose a prominent multi-decadal oscillation to the shear, but no significant trend was detected between 2000-2020 (Fig. 3d, dashed black line). In contrast, the interannual-to-decadal abyssal shear variability, and consequently the AABW transport variability, is mainly explained by the density variations at the DWBC with smaller but significant contributions from the western flank of MAR (Figs. 3c-3d). The variability at the DWBC explains approximately 80% of the detrended shear variance, generating shear anomalies that are highly correlated with the observed total shear anomalies (Extended Data, Fig. 1).

Like the shear and transport trends, the warming trend near the MAR is statistically significant below 4600 m, and its magnitude increases with depth, reaching rates of about 1.50 ± 0.25 m°C year^{-1} near 5000 m (green line in Fig. 3b). Additionally, downward isopycnal heaving is the mechanism responsible for warming, further suggesting the weakening of the AABW flow is associated with the shrinking of this bottom water layer (red line in Fig. 3b). Notably, cooling along isopycnal surfaces (aka, spice trend) indicates that the AABW has also freshened during the same period, surpassing the heaving effect above 4500 m (blue line in Fig. 3b). The average freshening rate of the AABW layer is approximately -2 ± 1×10^{-4} yr^{-1}.

The North Atlantic Abyssal Warming

As a result of the weakening of the relatively cold and fresh AABW flow since 2000, we expect the AABW layer to shrink, warming the abyssal North Atlantic as the overlaying NADW layer vertically expands [20]. To verify this, we use the hydrographic measurements obtained between 1998-2022 from multiple programs crossing the western North Atlantic basin between 24.5°N-26.5°N (Figs. 1 and 4). Like at 16°N, the AABW layer is primarily found below 4500 m with upwards tilted isotherms encroaching on the western flank of the MAR (Fig. 4a). In contrast, the AABW layer is significantly warmer at this latitude (i.e., average minimum temperatures ~0.2°C warmer), probably due to the continuous vertical mixing with NADW as it flows northward [26, 35]. Note that west of 69°W, the AABW layer thickness substantially decreases, resulting in the 1.8°C isotherm lying close to the bottom west of 72°W consistent with the presence of the DWBC and its localized recirculation cell carrying NADW in this area [38].

As seen at 16°N, the AABW is warming below approximately 4500 m on average (Fig. 4b). However, the trend only becomes statistically significant near ~5200 m (solid green line). Within the AABW layer (4500-6000 m), we estimate the average warming to be approximately 0.96 ± 0.56 m°C year^{-1}, which is driven by the downward heaving of the isopycnals (dashed red line). Because of the limited data covering the entire western North Atlantic basin (i.e., six cruises), the trend uncertainties are larger at this latitude (shaded area). To further validate this warming trend, we analyzed temperature variations over a smaller mid-basin section where several Deep Argo profiles were available and approximately evenly distributed along the CTD line. The trends over this smaller section that combines CTD and Argo profiles (solid orange line in Figs. 4b and

4c) are slightly different but consistent with the signal averaged over the AABW domain, resulting in an AABW layer warming rate of ~1 m°C year^{-1}.

Note that the abyssal western North Atlantic subtropics at 24.5°N-26.5°N seems to have cooled in 2020 (Figs. 4c-4e). Coincidentally, the AABW transport sharply increased between 2016-2017 across 16°N and remained relatively strong until 2020 (see Fig. 2b) compared to previous years when observations along 24.5°N-26.5°N were available, suggesting the AABW's transport interannual variability is likely responsible for the cooling. The temperature mooring records at 16°N also indicate a concurrent cooling below 4500 m (Extended Data, Fig. 2).

The moored and CTD measurements near the lateral edges of the AABW layer do not show a statistically significant trend (Figs. 4d-4e). Instead, shorter time scales dominate the temperature variability, suggesting the abyssal long-term warming is more robust closer to the core of the AABW. This spatial confinement of the warming signal could partially explain the inconsistent post-2000 temperature trends sign for broader areas of the abyssal North Atlantic estimated by previous studies [10, 27], since it includes regions with larger fractions of NADW (e.g., western boundary, areas east of MAR, depths between 4000-4500 m). Along the 24.5°N-26.5°N section, however, the inclusion of the hydrographic stations closer to the western boundary does not change the overall magnitude of the trend below 4500 m but instead significantly increases its uncertainties due to the spatial temperature variability.

Assuming the horizontally-averaged constant AABW warming rate profile (green line in Fig. 4b), we estimate the western North Atlantic gained about 0.49 ZJ between 2000-2020, equivalent to a 0.05 W m^{-2} heat flux across 4500 m between the Equator and 40°N (i.e., northernmost AABW penetration), contributing to a sea level rise (s) of 0.14 mm year^{-1} via thermal expansion (calculation details in Methods). Our western North Atlantic SLR estimates are consistent with the magnitude of the deep and abyssal warming contributions to global SLR from repeated hydrography since the 1990s [6, 27], which are at least one order of magnitude smaller than the upper ocean contribution to global long-term SLR trends [27]. One should interpret these numbers as a first-order rough approximation of the abyssal warming impact on the North Atlantic since our data do not include any latitudinal variability of the temperature trends. Nevertheless, the same average warming trend applied over 20 years results in a reduction of the climatological AABW layer volume of approximately $1.7 \pm 1.0 \times 10^{14}$ m^3 north of 16°N, which agrees within

uncertainties with the volume reduction suggested by the independent AABW transport estimates across 16°N (i.e., $1.1 \pm 0.4 \times 10^{14}$ m^3). In addition, [6] showed that the abyssal western North Atlantic (z>4000 m) gained heat at a similar rate between the early 1990s and early 2000s (i.e., 0.05 ± 0.18 W m^{-2}) using all available hydrographic data across the basin. However, the authors estimated an uncertainty three times the warming signal. Our rough heat flux estimates further corroborate these previous long-term trend estimates and suggest the trends pre- and post-2000 are similar.

The Persistent Abyssal AMOC Weakening

We showed that the northward flowing AABW across 16°N is mainly constrained below 4500 m and concentrated along the western flank of the MAR with a mean transport of 2.40 ± 0.25 Sv. This flow has weakened by approximately 0.35 Sv (i.e., 12%) between 2000-2020, associated with an average abyssal warming of about 1 m°C $year^{-1}$ driven by the downward heaving of the abyssal isopycnals within the AABW layer. Additionally, the AABW transport variability presents substantial interannual-to-decadal oscillations.

While we found AABW flow patterns at 16°N that are in general agreement with previous studies across the North Atlantic [26, 31, 35, 39], our analysis also revealed that the long-term weakening of the AABW inflow to the western North Atlantic since the 1980s [9, 26] persisted up to 2020, contributing to the increase of the abyssal heat content and, hence, sea-level rise in the region. As we mentioned earlier, multiple studies have reported AABW cooling in the North Atlantic in the 21st century [27, 31, 40] instead of warming. These conflicting reports result from relatively short time series and the inclusion of areas with significant NADW content in their analyses, reflecting the NADW variability [10, 27, 41].

Abyssal Ocean Circulation in a Warming Planet

The consistently observed contraction of the AABW layer along the main Atlantic AABW pathway (i.e., from the Weddell Sea through the Argentine, Brazil, and western North Atlantic basins) [3, 15, 17, 32, 42] together with the confirmation of the weakening of the abyssal geostrophic flow [this study] strongly suggests that these are effects of reduction in the AABW production and export rates around and out of the Southern Ocean, respectively. This observational-only perspective of the phenomenon further corroborates the numerical results

broadly explored in the past decades [18, 20, 25]. These numerical studies also showed that AABW anomalies are communicated northward on time scales shorter than abyssal advective time scales via wave propagation, suggesting the global abyssal circulation could rapidly adjust to a warmer planet in only a few decades.

Assuming the AABW spreading pathway between the Weddell Sea and 16°N between the Atlantic's western continental margins and western flank of MAR (≥13,000 km) and advective velocities between the maximum and average AABW flow speeds O(10^{-3}-10^{-2} m s^{-1}) (e.g., Fig. 1c and 2a), we expect advective time scales varying between 40-400 years, implying that anomalies from 1960s would only arrive in the North Atlantic subtropics in the early 2000s if advected at maximum AABW speeds. Although it is still unclear whether the production of AABW [25, 42] in or processes decreasing the AABW export out of [43] the Weddell Sea is dominating the downstream abyssal AMOC weakening [23], the flow weakening happening since the 1980s [3, 26] likely arrived in the North Atlantic Ocean through fast propagating topographic and planetary waves [20].

Notably, recent projections of the AABW flow reduction under the IPCC's high greenhouse gas emission scenarios suggest it could increase the global abyssal heat content by 10 ZJ between 1990-2050 [25]. Under the current warming rates, our results suggest around 10-15% of this excess heat could be in the abyssal western North Atlantic alone by 2050. Despite the relevance of the abyssal North Atlantic to the global heat budget, we report warming rates that are approximately half the trends observed below 4500 m throughout the western South Atlantic and parts of the Southern Ocean [14, 15, 24, 32, 44]. This difference is likely due to the continuous vertical mixing between the AABW and NADW along their pathways, especially over the rough topography of the MAR's western flank where both vertical mixing [35, 45, 46] and AABW flow are stronger (Fig. 1c). Therefore, to accurately predict the AABW evolution and the abyssal ocean's contribution to Earth's heat and carbon budgets, climate models must accurately represent the abyssal water's subtle properties variations and account for the impact of small-scale motions on the large-scale flow.

Acknowledgments

We thank the many scientists, engineers, and mariners from many institutions worldwide who supported several projects that developed instruments and collected, processed, and published the data we used in this work. That includes all CTD, Deep Argo, and moored profiles. Without their collaboration and hard work, studies like this would not happen. Especial thanks to Matthias Lankhorst and the MOVE team for providing the MOVE dataset, to the WBTS team (Ryan Smith, Denis Volkov, Rigoberto Garcia, James Hooper) for providing the WBTS mooring and CTD dataset, to Christopher Meinen, Matthew Harrison, Denis Volkov, Matthieu Le Henaff, and Leah Chomiak for the useful discussions. We also thank Sang-Ki Lee for reading the manuscript and providing useful comments. T.C.B., R.P., and S.D. gratefully acknowledge the funding from the NOAA's Global Ocean Monitoring and Observing program (FundRef number 100007298); NOAA's Climate Program Office, Climate Observations and Monitoring, and Climate Variability and Predictability programs under NOFO NOAA-OAR-CPO-2021-2006389 with additional NOAA Atlantic Oceanographic and Meteorological Laboratory support. Support for W.J.'s participation in the research was provided by the U.S. National Science Foundation under grants OCE-1332978 and OCE-1926008. T.K. is funded by the EU's Horizon 2020 Research and Innovation Program under the Grant agreement number 821001 (SO-CHIC), and therein is a contribution to its Work Packages 3 and 6. This study is further a contribution to the project T3 of the Collaborative Research Centre TRR 181 "Energy Transfers in Atmosphere and Ocean" funded by the Deutsche Forschungsgemeinschaft (DFG, German Research Foundation; project number 274762653). This research was carried out in part under the auspices of the Cooperative Institute for Marine and Atmospheric Studies, a cooperative institute of the University of Miami and the National Oceanic and Atmospheric Administration (NOAA), cooperative agreement NA 20OAR4320472.

Authors Contributions

- T.C.B. led this study from the idea conception to the data analysis, results interpretation, and manuscript writing.
- R.P. and S.D. contributed to the idea conception, results interpretation, discussion, and manuscript preparation.
- W.J. and T.K. contributed to the data analysis, results interpretation and discussion, and manuscript preparation.

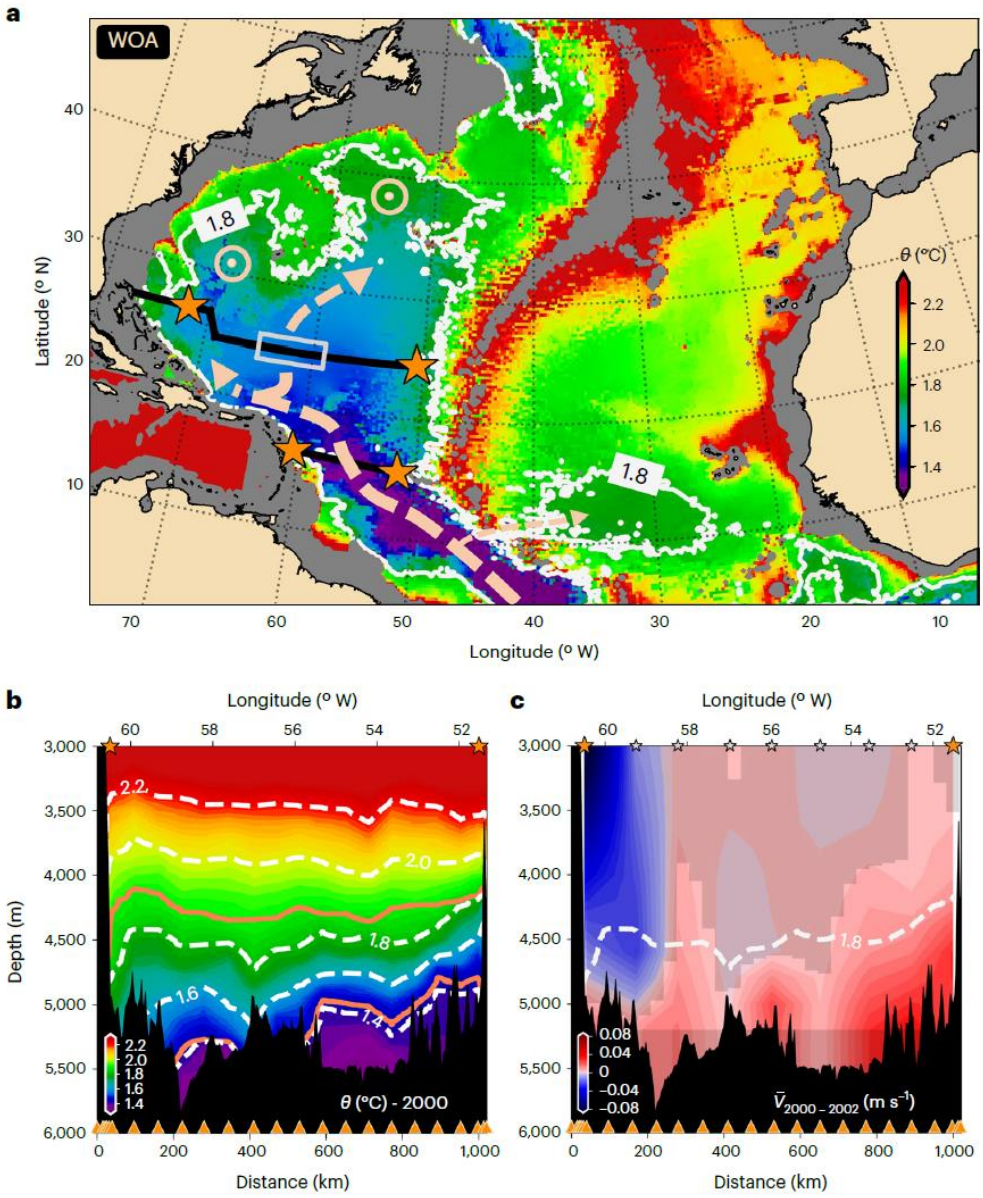

Fig. 1 Antarctic Bottom Water distribution and its primary pathways in the North Atlantic. (a) WOA potential temperature θ values closest to the bottom of the North Atlantic tropical and subtropical regions overlayed with the AABW flow (i.e., θ <1.8°C) direction and deep upwelling areas based on [29] (dashed arrows and circles, respectively). The stars indicate the mooring locations from the MOVE (16°N), RAPID (24.5°N), and WBTS (26.5°N) programs. The black line along 16°N represents the CTD transects from the MOVE program and where the GAGE moorings were also located. The black line farther north is the approximate location of the WOCE-GOSHIP CTD transects (i.e., A05 line). The gray box bounds the mid-basin area where Deep Argo profiles are present along 24.5°N (65°W-59°W). Areas shallower than 3000 m have been masked in gray. **(b)** Abyssal θ transect (color scales and dashed lines) obtained during the MOVE moorings (orange stars) deployment cruise in 2000 at 16°N, overlayed with γ_n = 28.110 and 28.135 kg m^{-3} isopycnals (solid orange lines). **(c)** Cross-transect 2000-2002 mean velocity from the GAGE program overlayed with θ = 1.8°C isotherm from the MOVE 2000 cruise (dashed white line). The dark shade indicates the areas where the uncertainty of the mean velocity surpasses the signal within the 95% confidence interval (i.e., 2×Standard Error; Sample Size = 403). Positive velocities are northward. Orange stars and triangles in **b** and **c** represent the MOVE moorings and CTD casts locations at 16°N, respectively. Gray and orange stars in **c** are the GAGE moorings locations.

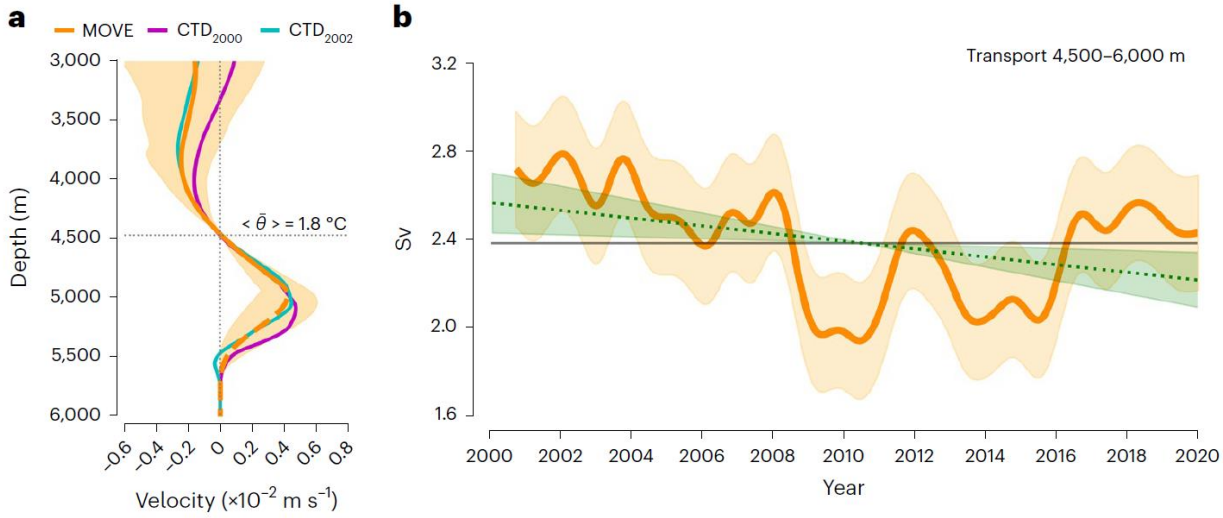

Fig. 2 MOVE data analysis showing the Antarctic Bottom Water flow weakening in the 21st century at 16°N. **(a)** Mooring-based 2000-2020 mean (orange line) and CTD-based (magenta and cyan lines) geostrophic velocity profiles between the MOVE moorings referenced at 4500 m. Positive velocities are northward. The dashed portion of the mooring-based profile shows where our vertical extrapolation scheme was applied. The shaded area is the mooring-based geostrophic velocity data range throughout the time series at each depth (Sample Size = 7341 data points). Finally, the horizontal dotted line is the average depth of the 1.8°C isotherm ($<\theta>$) calculated from the CTD transects. **(b)** Eighteen-month low-passed filtered AABW geostrophic transports referenced at and integrated between 4500-6000 m. The solid and dotted lines are the mean transport and the transport linear trend, respectively. Shaded areas around the curves represent the transport and its linear trend uncertainties within 95% confidence intervals of our calculations (i.e., 2×Standard Error). While the linear trend uncertainty was calculated using all 7341 data points, the standard errors of the transport correspond to the standard errors within a one-year-long running window (i.e., 365 data points).

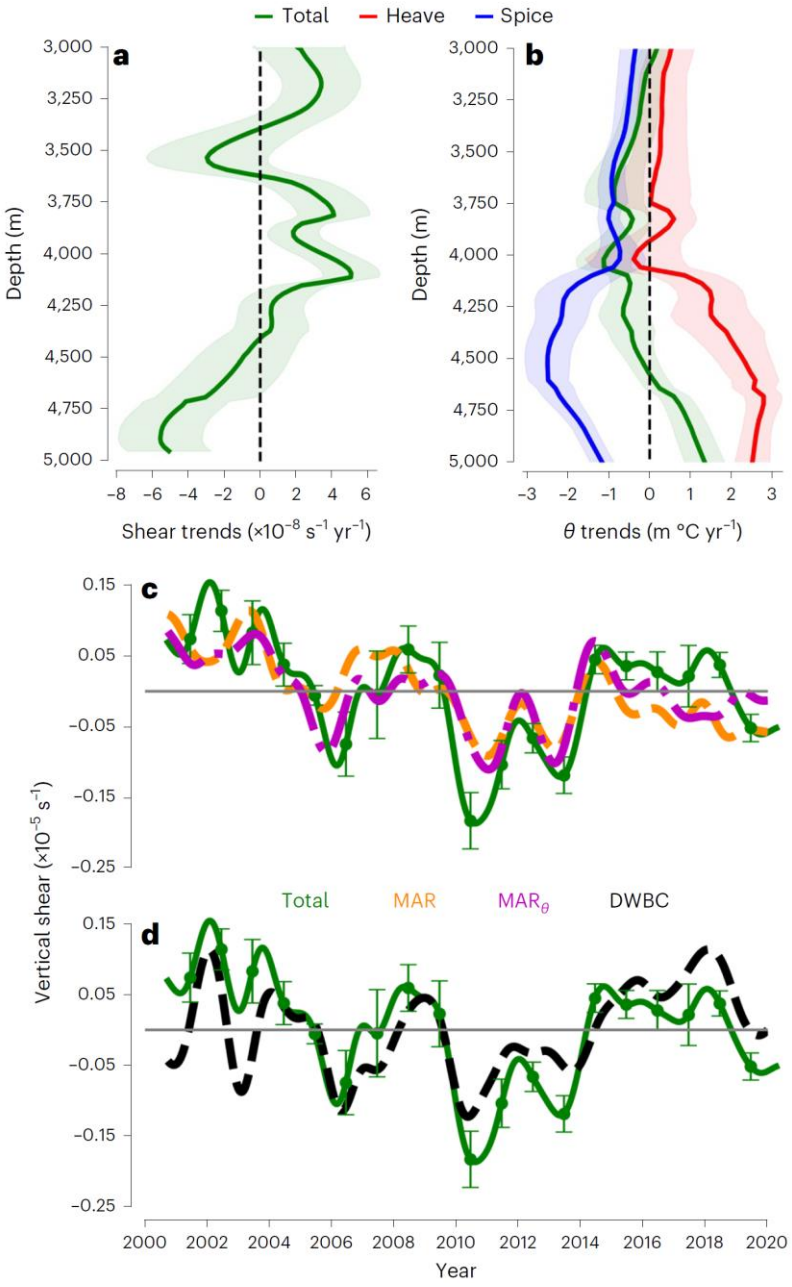

Fig. 3 MOVE data analysis showing that warming due to isopycnal heaving near the Mid-Atlantic Ridge decreased the abyssal geostrophic shear at 16°N. (a) The 2000-2020 linear geostrophic shear trends. **(b)** The 2000-2020 linear θ trends (green line) near the MAR and their decomposition into heave (red line) and spice (blue line) components. **(c)-(d)** Eighteen-month low-passed filtered abyssal geostrophic shear time anomalies averaged between 4500-5000 m (solid green line) and its correspondent variability sources: density changes near the MAR (orange dashed line), temperature changes near the MAR (MAR_θ, magenta dashed line), and density changes within the DWBC domain (DWBC, dashed black line). The sum of MAR and DWBC curves corresponds to the Total shear. Uncertainties, shown as shaded areas and error bars, represent the 95% confidence intervals (2×Standard Error) around each curve. While the linear trends' uncertainties in **a** and **b** were calculated using all 7341 data points, the vertical shear standard errors in **c** and **d** correspond to the standard errors within a one-year-long running window (i.e., 365 data points).

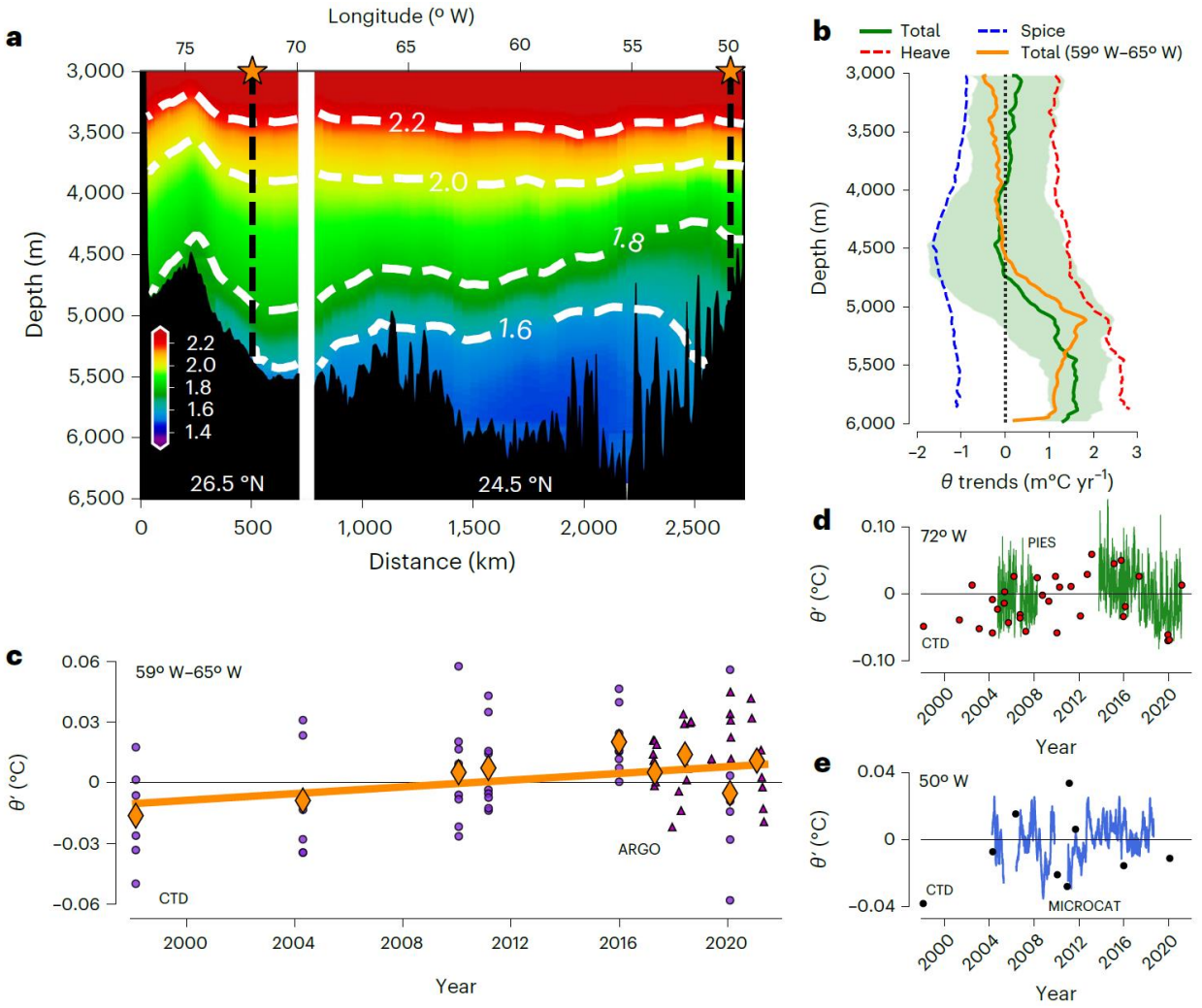

Fig. 4 Analysis of the hydrographic observations showing the Antarctic Bottom Water distribution and its warming signal at 24.5°N-26.5°N. (a) Abyssal mean θ transect calculated from CTD casts obtained as part of the WBTS, WOCE-GOSHIP, and RAPID programs between 1998 and 2020. Stars and dashed black lines indicate the WBTS' moored PIES (72°W) and the RAPID moored MicroCATs (50°W) locations. **(b)** CTD-based linear θ trends averaged across the basin along 24.5°N (solid green line), and its heave and spice components (red and blue dashed lines, respectively) overlayed with CTD+Argo-based linear θ trends between 1998-2022 near the center of the basin (59°W-65°W, solid orange line). The shaded area represents the 95% confidence interval of the basin-wide total trend (i.e., 2×Standard Error; Sample Size = 6 data points). **(c)** Vertically-averaged θ anomalies below 4500 m depth near the center of the basin (59°W-65°W) from CTD casts (small circles) and Argo profiles (small triangles). While the thick solid orange line shows the warming trend obtained by combining CTDs and Argo measurements, the large diamonds represent the zonally averaged temperature measurements. **(d)-(e)** Near bottom θ anomalies at the western and eastern edges of the AABW layer from moored records and CTD casts at the moorings' sites. Note that the y-axis limits are panel-dependent for better visualization.

References

[1] Orsi, A. H., Johnson, G. C. & Bullister, J. L. Circulation, mixing, and production of Antarctic Bottom Water. *Prog. Oceanog.* **43**, 55–109 (1999). https://doi.org/10.1016/S0079-6611(99)00004-X .

[2] Lumpkin, R. & Speer, K. Global Ocean Meridional Overturning. *J. Phys. Oceanogr.* **37**, 2550–2562 (2007). https://doi.org/10.1175/JPO3130.1 .

[3] Johnson, G. C. Quantifying Antarctic Bottom Water and North Atlantic deep water volumes. *J. Geophys. Res.* **113**, C05027 (2008). https://doi. org/10.1029/2007JC004477 .

[4] Johnson, G. C. *et al.* Blunden, J., Arndt, D. S. & Hartfield, G. (eds) *Global oceans: Ocean heat content*. (eds Blunden, J., Arndt, D. S. & Hartfield, G.) *Bull. Amer. Meteor. Soc.*, Vol. 99, Si–S310 (2018).

[5] Bagnell, A. & DeVries, T. 20th century cooling of the deep ocean contributed to delayed acceleration of Earth's energy imbalance. *Nat. Commun.* **12**, 4604 (2021). https://doi.org/10.1038/s41467-021-24472-3 .

[6] Purkey, S. G. & Johnson, G. C. Warming of global abyssal and deep Southern Ocean waters between the 1990s and 2000s: Contributions to global heat and sea level rise budgets. *J. Climate* **23**, 6336–6351 (2010). https://doi.org/10.1175/2010JCLI3682.1 .

[7] Kouketsu, S. *et al.* Deep ocean heat content changes estimated from observation and reanalysis product and their influence on sea level change. *JGR* **116**, C03012 (2011). https://doi.org/10.1029/2010JC006464 .

[8] Zenk, W. & Morozov, E. Decadal warming of the coldest Antarctic Bottom Water flow through the Vema Channel. *Geophysical Research Letters* **34**, L14607 (2007). https://doi.org/10.1029/2007GL030340 .

[9] Johnson, G. C., Purkey, S. G. & Toole, J. M. Reduced Antarctic meridional overturning circulation reaches the North Atlantic Ocean. *Geophys. Res. Lett.* **35**, L22601 (2008). https://doi.org/10.1029/2008GL035619 .

[10] Desbruyères, D. G., Purkey, S. G., McDonagh, E. L., Johnson, G. C. & King, B. A. Deep and abyssal ocean warming from 35 years of repeat hydrography. *Geophys. Res. Lett.* **43**, 10,356–10,365 (2016). https://doi. org/10.1002/2016GL070413 .

[11] Menezes, V. V., Macdonald, A. M. & Schatzman, C. Accelerated freshening of Antarctic Bottom Water over the last decade in the southern indian ocean. *Sci. Adv.* **3** (2017). https://doi.org/10.1126/sciadv.1601426 .

[12] Purkey, S. G. *et al.* Unabated bottom water warming and freshening in the South Pacific Ocean. *J. Geophys. Res-Oceans* **124**, 1778–1794 (2019). https://doi.org/10.1029/2018JC014775 .

[13] Johnson, G. C., Purkey, S. G., Zilberman, N. V. & Roemmich, D. Deep Argo quantifies bottom water warming rates in the southwest Pacific Basin. *Geophys. Res. Lett.* **46**, 2662–2669 (2019). https://doi.org/10. 1029/2018GL081685 .

[14] Strass, V. H., Rohardt, G., Kanzow, T., Hoppema, M. & Boebel, O. Multi-decadal warming and density loss in the deep Weddell Sea, Antarctica. *J. Climate* **33**, 9863–9881 (2020). https://doi.org/10.1175/JCLI-D-20-0271.1 .

[15] Johnson, G. C. Antarctic Bottom Water Warming and circulation slow-down in the Argentine Basin from analyses of deep Argo and historical shipboard temperature data. *Geophys. Res. Lett.* **49** (2022). https://doi.org/10.1029/2022GL100526 .

[16] van Wijk, E. M. & Rintoul, S. R. Freshening drives contraction of Antarctic Bottom Water in the Australian Antarctic Basin. *Geophys. Res. Lett.* **41**, 1657–1664 (2014). https://doi.org/10.1002/2013GL058921 .

[17] Purkey, S. G. & Johnson, G. C. Global contraction of Antarctic Bottom Water between the 1980s and 2000s. *J. Climate* **25**, 5830–5844 (2012). https://doi.org/10.1175/JCLI-D-11-00612.1 .

[18] Masuda, S. *et al.* Simulated rapid warming of abyssal North Pacific waters. *Science* **329**, 319–322 (2010). https://doi.org/10.1126/science.1188703 .

[19] Nakano, H. & Suginohara, N. Importance of the eastern Indian Ocean for the abyssal Pacific. *J. Geophys. Res-Oceans* **107**, 3219 (2002). https://doi.org/10.1029/2001JC001065 .

[20] Patara, L. & B¨oning, C. W. Abyssal ocean warming around Antarctica strengthens the Atlantic overturning circulation. *Geophys. Res. Lett.* **41**, 3972–3978 (2014). https://doi.org/10.1002/2014GL059923 .

[21] Khatiwala, S., Primeau, F. & Holzer, M. Ventilation of the deep ocean constrained with tracer observations and implications for radiocarbon estimates of ideal mean age. *Planet. Sci. Lett.* **325-326**, 116–125 (2012). https://doi.org/10.1016/j.epsl.2012.01.038 .

[22] Solodoch, A. *et al.* How does Antarctic Bottom Water cross the Southern Ocean? *Geophys. Res. Lett.* **49** (2022). https://doi.org/10.1029/ 2021GL097211 .

[23] Silvano, A. *et al.* Observing Antarctic Bottom Water in the Southern Ocean. *Front. Mar. Sci.* **10** (2023). https://doi.org/10.3389/fmars.2023. 1221701 .

[24] Campos, E. J. D. *et al.* Warming trend in Antarctic Bottom Water in the Vema Channel in the South Atlantic. *Geophys. Res. Lett.* **48** (2021). https://doi.org/10.1029/2021GL094709 .

[25] Li, Q., England, M. H., Hogg, A. M., Rintoul, S. R. & Morrison, A. K. Abyssal ocean overturning slowdown and warming driven by Antarctic meltwater. *Nature* **615**, 841–847 (2023). https://doi.org/10.1038/ s41586-023-05762-w .

[26] Frajka-Williams, E., Cunningham, S. A., Bryden, H. & King, B. A. Variability of Antarctic Bottom Water at 24.5°N in the Atlantic. *J. Geophys. Res-Oceans* **116** (2011). https://doi.org/10.1029/2011JC007168 .

[27] Desbruy`eres, D., McDonagh, E. L., King, B. A. & Thierry, V. Global and full-depth ocean temperature trends during the early twenty-first century from Argo and repeat hydrography. *J. Climate* **30**, 1985–1997 (2017). https://doi.org/10.1175/JCLI-D-16-0396.1 .

[28] Schmitz, W. J. & McCartney, M. S. On the North Atlantic circulation. *Rev. Geophys.* **31**, 29–49 (1993). https://doi.org/10.1029/92RG02583 .

[29] Talley, L. D., Pickard, G. L., Emery, W. J. & Swift, J. H. *Descriptive physical oceanography: an introduction* sixth edn (Academic Press, London, 2011).

[30] Herrford, J., Brandt, P. & Zenk, W. Property changes of deep and bottom waters in the western tropical Atlantic. *Deep Sea Res. Part I Oceanogr. Res. Pap.* **124**, 103–125 (2017). https://doi.org/10.1016/j.dsr.2017.04.007 .

[31] Cunningham, S. A. & Alderson, S. Transatlantic temperature and salinity changes at 24.5°N from 1957 to 2004. *Geophys. Res. Lett.* **34** (2007). https://doi.org/10.1029/2007GL029821 .

[32] Johnson, G. C., Cadot, C., Lyman, J. M., McTaggart, K. E. & Steffen, E. L. Antarctic Bottom Water warming in the Brazil Basin: 1990s through 2020, from WOCE to deep Argo. *Geophys. Res. Lett.* **47** (2020). https://doi.org/10.1029/2020GL089191 .

[33] Johnson, G. C., Robbins, P. E. & Hufford, G. E. Systematic adjustments of hydrographic sections for internal consistency. *J. Atmos. Oceanic Technol.* **18**, 1234–1244 (2001). https://doi.org/10.1175/1520-0426(2001) 018⟨1234:SAOHSF⟩2.0.CO;2 .

[34] Wright, W. R. Northward transport of Antarctic Bottom Water in the western Atlantic Ocean. *Deep-Sea Res.* **17**, 367–371 (1970). https://doi. org/10.1016/0011-7471(70)90028-8 .

[35] Mauritzen, C., Polzin, K. L., McCartney, M. S., Millard, R. C. & West-Mack, D. E. Evidence in hydrography and density fine structure for enhanced vertical mixing over the Mid-Atlantic Ridge in the western Atlantic. *J. Geophys. Res.* **107**, 3147 (2002). https://doi.org/10.1029/ 2001JC001114 .

[36] Kanzow, T. *Monitoring the integrated deep meridional flow in the tropical North Atlantic*. Ph.D. thesis, Christian-Albrechts Universit¨at Kiel, Germany (2004).

[37] Spall, M. A. Wave-induced abyssal recirculations. *J. Mar. Res.* **52**, 1051–1080 (1994). https://doi.org/10.1357/0022240943076830 .

[38] Biló, T. C. & Johns, W. E. The Deep Western Boundary Current and adjacent interior circulation at 24°–30°N: Mean structure and mesoscale variability. *J. Phys. Oceanogr.* **50**, 2735–2758 (2020). https://doi.org/10. 1175/JPO-D-20-0094.1 .

[39] Kanzow, T., Send, U., Zenk, W., Chave, A. D. & Rhein, M. Monitoring the integrated deep meridional flow in the tropical North Atlantic: Long-term performance of a geostrophic array. *Deep Sea Res. Part I Oceanogr. Res. Pap.* **53**, 528–546 (2006). https://doi.org/10.1016/j.dsr.2005.12.007 .

[40] Limeburner, R., Whitehead, J. A. & Cenedese, C. Variability of Antarctic bottom water flow into the North Atlantic. *Deep Sea Res. Part II Top. Stud. Oceanogr.* **52**, 495–512 (2005). https://doi.org/10.1016/j.dsr2.2004.12.012 .

[41] Desbruy`eres, D. G. *et al.* Warming-to-cooling reversal of overflow-derived water masses in the Irminger Sea during 2002–2021. *GRL* **49**, 1–10 (2022). https://doi.org/10.1029/2022GL098057 .

[42] Zhou, S. *et al.* Slowdown of Antarctic Bottom Water export driven by climatic wind and sea-ice changes. *Nat. Clim. Change* **13**, 701–709 (2023). https://doi.org/10.1038/s41558-023-01695-4 .

[43] Meredith, M. P., Garabato, A. C. N., Gordon, A. L. & Johnson, G. C. Evolution of the deep and bottom waters of the Scotia Sea, Southern Ocean, during 1995–2005. *J. Climate* **21**, 3327–3343 (2008). https://doi.org/10.1175/2007JCLI2238.1 .

[44] Meinen, C. S., Perez, R. C., Dong, S., Piola, A. R. & Campos, E. J. D. Observed ocean bottom temperature variability at four sites in the northwestern Argentine Basin: evidence of decadal deep/abyssal warming amidst hourly to interannual variability during 2009–2019. *Geophys. Res. Lett.* **47** (2020). https://doi.org/10.1029/2020GL089093.

[45] Polzin, K. L., Toole, J. M., Ledwell, J. R. & Schmitt, R. W. Spatial variability of turbulent mixing in the abyssal ocean. *Science* **276**, 93–96 (1997). https://doi.org/10.1126/science.276.5309.93 .

[46] St Laurent, L. C. & Thurnherr, A. M. Intense mixing of lower thermocline water on the crest of the Mid-Atlantic Ridge. *Nature* **448**, 680–683 (2007). https://doi.org/10.1038/nature06043.

Methods

Mooring records

To study the AABW inflow (i.e., transport) to the subtropical North Atlantic, we analyzed data from two hydrographic moorings between February 2000 and December 2020 from the Meridional Overturning Variability Experiment (MOVE) at 16°N [47]. These moorings provide measurements down to 5000 m depth near the western boundary and the western flank of the MAR (Fig. 1, Supplemental Information Fig. S1, and Table S1). In addition, to aid in the interpretation of the results and the transport calculations across 16°N, we used nine Guyana Abyssal Gyre Experiment (GAGE) current meter moorings deployed between the MOVE moorings [39, 48]. The GAGE observations are located between ~1600-5200 m of the water column and range from February 2000 to April 2002 (Fig. 1c, Supplemental Information Fig. S1, and Table S2). Then, to interpret temperature variability in the North Atlantic subtropics, we analyzed near-bottom (~5000 m) temperature records at two additional locations farther north (24.5°N-26.5°N) at the MAR's western flank and near the western boundary (Figs. 1a, 4a, and Supplemental Information Table S3). At MAR's western flank, we used temperature, conductivity, and pressure records between April 2004 and August 2018 from a mooring from the Rapid Climate Change Meridional Overturning Circulation program (RAPID) [49, 50]. Near the western boundary, temperature records between September 2004 and March 2021 were from a Pressure Equipped Inverted Echo Sounder's (PIES) internal temperature sensor. The PIES' records were obtained from the Western Boundary Current Time Series (WBTS) program [51]. Details about the datasets and data accuracy can be found in the Support Information under Moored Instrumentation.

Cruise hydrographic data and auxiliary data products

We utilized quality-controlled hydrographic CTD, Deep Argo, and climatological profiles from various sources to map the AABW layer and study the abyssal temperature variability. At 16°N, we relied on CTD profiles from two cruises initiated in February 2000 and 2002 servicing the MOVE and GAGE moorings [48] (Figs. 1b-1c). Along 24.5°N-26.5°N latitudes, we analyzed CTD profiles from six occupations of the transatlantic historical A05 line between 1998-2020 that started as part of the World Ocean Circulation Experiment (WOCE) and continued under the coordination of the International Global Ocean Ship-Based Hydrographic Investigations Program (GOSHIP). Additionally, we included 28 CTD transects repeated between 2000 and 2021,

spanning 70°W-77°W along 26.5°N as part of the WBTS program [51], and profiles from seven cruises servicing the RAPID mooring on the western flank of the MAR since 2004 (see Fig. 1a for the area covered by the observations). To strengthen our CTD data analysis, we also used a total of 36 Argo quality-controlled temperature and salinity profiles from deep Argo floats [52] obtained between March 2017 and May 2021 as additional abyssal potential temperature measurements (see gray box in Fig. 1a for reference). These floats take measurements down to a depth of 6000 m. Further details about these datasets and their respective accuracy can be found in the Support Information under CTD Measurements Accuracy and Deep Argo Data.

Finally, we analyzed the climatological temperature and salinity within the abyssal North Atlantic from the World Ocean Atlas (WOA) 2018 product [53, 54]. This product has a horizontal resolution of 0.25°×0.25°, global coverage, and 102 vertical levels ranging from 0-5500 m depth. The topography data displayed and mentioned throughout this article is the General Bathymetric Chart of the Oceans (GEBCO) 30-arc second resolution gridded topographic product [55].

Geostrophic shear and AABW transports at 16°N

In the North Atlantic, the AABW is commonly defined as waters within the potential temperature layer colder than 1.8°C [9, 26, 56]. To assess the AABW flow variability, we estimated the geostrophic volume transport of waters within this cold layer at 16°N across the MOVE array (Fig. 1) between 2000-2020. We chose 16°N due to the high-temporal resolution of the MOVE array measurements (i.e., 5-10 minutes) compared to other available datasets. This way, we avoid aliasing problems of transport variability analysis on subinertial time scales. It is worth mentioning that we do not attempt to estimate the AABW transports using the GAGE moorings because the array was not designed to resolve the lateral structure of the boundary currents at 16°N, compromising absolute transport estimates from directly observed velocities [36].

To do this, we first vertically interpolated the temperature and salinity measurements at each MOVE mooring location using the Piecewise Cubic Hermite Interpolating Polynomial [57] to a uniform 20 m grid. Throughout the consistent 13 MOVE deployments (Supplemental Information Table S1), this procedure allowed us to obtain temperature and salinity at the same depths in both locations between 2000 and 2020 and vertically interpolate over short data gaps generated by sporadic instrument failures. Then, we computed the dynamic height profiles at each mooring

location, allowing us to use the Dynamic Method [29] to estimate the zonally averaged geostrophic velocity profile (i.e., net geostrophic flow profile) relative to 4500 m between the two moorings. The 4500 m level represents the average depth of the approximate NADW-AABW interface at 16°N (i.e., 1.8°C isotherm). Finally, we performed a vertical extrapolation to obtain the flow below 5000 m before integrating the velocity between the moorings and below 4500 m (see section "The vertical extrapolation below 5000 m" for details).

After obtaining a complete 4500 m-bottom zonally averaged geostrophic velocity profile at each time step, we computed the horizontally-integrated transport by multiplying the velocity by the average distance between the MOVE moorings (i.e., ~1000 km). Then, we vertically integrated this transport below 4500 m using a trapezoidal integration scheme to obtain the final AABW transports across 16°N in Sverdrups (i.e., 1 Sv = 1×10^6 m^3 s^{-1}).

The referencing at 4500 m

The northward AABW flow opposes the southward NADW flow within lighter and warmer layers of the water column [29, 56]. Therefore, we chose the commonly assumed NADW-AABW interface in the North Atlantic– i.e., 1.8°C isotherm mean depth of 4500 m – as the reference level to obtain the closest geostrophic velocities to the ocean's absolute velocity as possible at 16°N. However, accurately estimating the mean 1.8°C isotherm depth based solely on the mooring data was difficult due to the approximately 1000 km distance between the moorings (Fig. 1b). To address this issue, we used high-resolution CTD transects obtained during 2000 and 2002 cruises servicing the MOVE and GAGE moorings. Based on these cruises, we found that the average depth of the 1.8°C isotherm between the MOVE moorings is approximately 4500 m (e.g., Fig. 1b), which is also supported by the WOA18 climatology at 16°N.

The referencing procedure corresponds to the primary source of uncertainty in geostrophic estimates [58]. Therefore, it is imperative to examine the referencing limitations and uncertainties. Previous analysis of the first few years of MOVE hydrographic records and the MOVE-GAGE current meter measurements obtained between 2000-2002 indicated that an average level of no motion could exist around 4300 m [36, 48]. Because 4300 m is relatively close to 4500 m compared to the thickness of the AABW layer (~4500-6000 m, see Figs. 1b and 1c), the mean average AABW transport and AMOC weakening referenced at ~4300 m agrees with our estimates within

uncertainties. In addition, the 4500 m corresponds to the average level of no motion from geostrophic estimates done within numerical simulations [59].

Although the AABW layer is mostly below 4500 m, a constant level of no motion has never been found in the real ocean. For example, under the current abyssal warming scenario, where the AABW layer is shrinking over the years [9], assuming a fixed level of no motion may not be appropriate since the depth of zero velocity may be deepening, resulting in a more substantial weakening of the transport. In the Supplemental Information (see Sensitivity Test for the Geostrophic Referencing at the Constant Depth of 4500 m at 16°N), our simple variability analysis of the 1.8°C isotherm depth shows that the relatively modest vertical motions of this interface (standard deviation of ∼47 m and trend of ∼1.4 m year^{-1}) do not impose substantial changes in the AABW transport trends or its variability on interannual time scales (Supplemental Information Fig. S2), highlighting the robustness of our results. In contrast, transport oscillations on shorter time scales are substantially impacted by the choice of a constant level of no motion, suggesting this method might not be suitable on daily-to-seasonal time scales. Finally, choosing a significantly deeper reference level can modify the transport variability characteristics in all time scales due to the proximity to the maximum AABW velocity (Supplemental Information Fig. S3). To conclude, for the purpose of this study, a constant 4500 m is a reasonable reference choice, given the evidence from the previous studies, the documented AABW boundaries at 16°N, and sensitivity analyses discussed in the Supplemental Information.

The vertical extrapolation below 5000 m

The MOVE array moorings do not observe areas deeper than 5000 m. According to the GEBCO topography and previously reported topographic data [39, 48, 59, 60], the average water column depth across the MOVE array is approximately 5400 m (Figs. 1a-1b), with a valley reaching almost 6000 m. Therefore, a significant portion of the abyssal flow is not directly observed by the MOVE array. Not resolving the full abyssal ocean is common for most AMOC monitoring arrays.

Notably, velocity distributions (Figs. 1c and 2a), previous analysis of moored records at 16°N [36, 48], and numerical estimates of the net flow across 16°N [59] suggest that the AABW maximum northward flow is located around 5000-5200 m. Therefore, since we observe the velocities near 5000 m, it is possible to estimate the unresolved transport assuming a realistic

velocity vertical shear below 5000 m. To estimate the abyssal shear and the unresolved transport, we determined the depth range over which the AABW net flow decays to zero using the GAGE current meter moorings and high-resolution CTD records. Then, we vertically interpolated the geostrophic profiles between the deepest MOVE measurement and this near-bottom zero velocity depth.

Like the MOVE moorings, the GAGE instruments do not cover the entire water column. However, because the GAGE observations largely overestimate the net AABW maximum velocities due to its well-known lateral resolution problem [36], we can extrapolate the current meter velocity profiles at each GAGE mooring location to obtain an overestimate of the net flow near the bottom and its vertical shear. We obtained an upper and lower limit for the shear below 5200 m by applying a Dirichlet (i.e., no-slip condition $v = 0$ m s^{-1} at the sea floor) and a Newman (i.e., full-slip condition $\partial v/\partial z = 0$ s^{-1} at the sea floor) velocity boundary conditions at the bottom. Supplemental Information Fig. S4 shows the horizontally averaged GAGE velocity profiles. For both conditions, the velocity profile decays to values below 1×10^{-3} m s^{-1} at approximately 5600 m and to virtually zero at 5800 m. Additionally, the geostrophic velocity profiles referenced at 4500 m from the high-resolution CTDs show similar velocity values at these depths with zero-velocity crossing depth at approximately 5700 m (Fig. 2a).

To determine the AABW transports from the MOVE array, we assumed constant zero crossing velocities at approximately 5700 m, with 100 m of uncertainty propagated across our transport calculations. We then used a shape-preserving spline scheme [61] to vertically interpolate the resulting geostrophic velocity profile for the final velocity integration. Note that our extrapolation scheme does not account for minor nuances in the geostrophic profiles below 5000 m, such as velocity sign inversions (Fig. 2a). However, the AABW transports obtained from both the 2000 (2.96 Sv) and 2002 (2.45 Sv) CTD-based transports fall within the 95% confidence interval of the average transport from the MOVE moorings. When comparing the CTD transect transport in 2002 with the concurrent MOVE mooring-based transport, the values agree within the uncertainties. Unfortunately, the CTD transect in 2000 was obtained before the MOVE array became fully operational, preventing us from directly comparing the CTD-based with the mooring-based transports.

The geostrophic shear variability decomposition

To assess the contributions of the hydrographic property variability to the long-term vertical geostrophic shear trend (Figs. 3c-3d), we calculated the shear time series at each depth due to the density changes near the MAR (MAR), temperature changes near the MAR (MAR_θ), and density changes within the DWBC domain (DWBC). To do so, we replaced the temperature and salinity time series with their respective constant 20-year-long time average as follows:

- **MAR:** Constant density profile at the western boundary mooring site.
- **MAR_θ:** Constant density profile at the western boundary mooring and constant salinity at the MAR mooring.
- **DWBC:** Constant density profile at the MAR mooring site.

Potential temperature trends decomposition, ocean heat content, and thermal expansion of the sea water

To quantitatively attribute the portion of the Potential Temperature (θ) trends associated with the isopycnal vertical displacements at each depth, we decomposed θ temporal anomalies into heave (i.e., θ anomalies at a fixed pressure due to isopycnal displacement) and spice (θ anomalies along density surfaces) [62]. Temperature profiles along the WOCE/GOSHIP A05 transect and from the MOVE mooring near the MAR were interpolated onto a 5×10^{-4} kg m^{-3} resolution neutral density (γ_n) vertical grid. Then we computed the heave and spice terms in density space following Eq. 1 [41, 63].

$$\theta' = \theta'\,|_{\gamma_n} + z' \times \frac{\partial \theta}{\partial z}\,|_{\gamma_n}, \tag{1}$$

where the first and second terms of the right-hand-side are the spice and heave components, respectively, and z is depth. The term $\partial\theta/\partial z$ is the background (i.e., time-averaged) thermal gradient. After we estimated the θ terms, we reinterpolated them to the original vertical depth coordinates such that temporal linear trends could be calculated.

To perform our rough estimates of the increase of the abyssal ocean heat content (ΔQ) and its contribution to sea level rise (SLR) between 2000-2020, we solved the well-known and widely used Eqs. 2 and 3 [6].

$$\Delta Q = \int_v \Delta\theta(z) \times \rho \times C_p \, dV, \tag{2}$$

where V is the AABW volume, ρ is the water density, C_p is the seawater's isobaric heat capacity, and $\Delta\theta(z)$ is the potential temperature change profile over 20 years.

$$\mathrm{SLR} = \frac{\int_v \Delta\theta(z)\times\alpha dV}{A}, \tag{3}$$

where α is the thermal expansion of the seawater and A is the North Atlantic area covered by AABW. All parameters from Eqs. 2 and 3 were calculated using the WOA18 climatology in the western North Atlantic, except the $\Delta\theta(z)$. We obtained AABW's area and volume based on the climatological distribution of the waters colder than 1.8°C (i.e., west of the MAR's crest). While the area corresponds to the areal extent of waters colder than 1.8°C, the volume was calculated as the sum of the AABW volume in each WOA18's grid cell with 0.25 × 0.25°of area. At each grid cell, the AABW thickness was defined as the distance between the 1.8°C isotherm and local bottom depth from GEBCO. Then we calculated the profile $\Delta\theta(z)$ by time integrating the CTD-based temperature trend profile at 24.5°N shown in Fig. 4b (green line) over 20 years. We obtained similar results by assuming a uniform average warming rate of ~1 m°C year^{-1} between 4500 m-bottom in the western North Atlantic south of 40°N (i.e., northernmost AABW penetration in Fig. 1a).

Seawater properties and dynamic height

We estimated all seawater parameters and properties (i.e., θ, ρ, C_p, α) and the dynamic height for the geostrophic estimates using the TEOS-10 Python Gibbs Seawater Oceanographic 3.4.2 software [64], except γ_n. Therefore, all properties and parameters were calculated as a function of Conservative Temperature and Absolute Salinity required by the TEOS-10 subroutines. We chose to show our results in terms of θ and Practical Salinity for a convenient comparison with previous studies and discussion of the results. Additionally, results from Eqs. 2 and 3 do not depend on the temperature scale in the abyssal ocean, being the ΔQ and SLR values several orders of magnitude larger than the difference between the results using the different temperature scales. Although the γ_n capabilities were discontinued from this particular Python package, the previous versions still have the γ_n calculation routines following [65]'s methodology.

Unfortunately, PIES and 18 of the Deep Argo profiles did not provide salinity records, so we cannot readily use the available software and data to estimate θ from these records. The former

does not have a conductivity sensor for salinity calculations, and the latter presents conductivity measurements below 4500 m flagged as bad or missing data by the quality control procedure [52]. Because the range of salinity values below 3000 m is small (34.84-34.89), assuming a constant salinity value to convert *in-situ* temperature records to θ results in errors smaller than 4×10^{-3} m°C below 4500 m, which is orders of magnitude smaller than the observed temperature variability. Therefore, to convert the PIES and Deep Argo *in-situ* temperature profiles in θ, we used the 3000-6000 m average salinity from the CTDs along A05 (see Supplemental Information under Estimating Potential Temperature).

Filtering procedure, computation of trends, and trends uncertainties

We isolated the interannual and longer time scales in our time series by low-pass filtering them. Our filtering procedure consists of a fourth-order Butterworth filter [66] with a cutoff period of 18 months [67]. In addition, we fitted linear models to our time series using standard unweighted least squares regressions [66] to estimate the AABW transport, velocity shear, and temperature trends.

Uncertainties and their respective confidence intervals discussed throughout this study represent the standard errors of each statistical parameter unless explicitly stated otherwise. For trends and low-pass filtering procedures, we calculated the standard errors using the distribution of the residuals between the original time series and the linear model, or filtered series [13, 41]. Finally, due to the vigorous interannual variability of the AABW geostrophic transport (Figs. 2b), its non-normal distribution (Fig. S5a and Table S4), and the presence of serial correlations in the series (Fig. S5b), additional trend estimate methods and significance tests are required to assess the robustness of our calculations further. Therefore, we used the pyMannKendall software [68] to apply different versions of the non-parametric Mann Kendall (MK) trends statistical tests [69-71] to quantify the robustness of our calculations. All tests suggested AABW transport trends are significant at the 95% confidence level with p-values smaller than 0.01 (Supplemental Information Table S5). Details about our error analyses and statistical tests can be found in the Supplemental Information under Uncertainties.

Data Availability

All data used in this study are freely available and can be accessed as follows: MOVE (link for the OceanSITES Global Data Assembly Center Public FTP Server can be found at https://mooring.ucsd.edu/move/, accessed on November 15th 2022); GAGE (https://doi.org/10.17604/5jd9-7f77, published on June 22, 2023); WOCE and GOSHIP A05 line (https://cchdo.ucsd.edu/, accessed on February 14, 2023); RAPID (https://www.bodc.ac.uk/data/ bodc database/nodb/, accessed on October 21, 2022); Deep Argo (https://www.seanoe.org/data/00311/42182/, accessed on February 27, 2024); WBTS (link for AOML-NOAA's public FTP server can be found at https://www.aoml.noaa.gov/phod/wbts/data.php, accessed on February 13, 2023); WOA18 (https://www.ncei.noaa.gov/data/oceans/woa/WOA18/ DATA/, accessed on January 10, 2023); GEBCO (https://www.gebco.net/ data and products/gridded bathymetry data/, accessed on April 9, 2021)

Code Availability

All the codes used in this study are freely available in public repositories. As mentioned in Methods, all relevant seawater parameters, properties, and dynamic height were computed using the Python Gibbs Seawater Oceanographic 3.4.2 software available at https://www.teos-10.org/software.htm#1. The γ_n routine can be found at http://www.teos-10.org/preteos10 software/ gamma GP.html. The Python pyMannKendall software for the MK trends statistical tests is available at https://github.com/mmhs013/pyMannKendall/ tree/v1.1. Finally, all data handling, mathematical operations, data interpolation, and data filtering procedures were performed using standard functions found in the Xarray 0.20.1 (https://docs.xarray.dev/en/stable/), Numpy 1.21.5 (https://numpy.org/), and Scipy 1.7.3 (https://scipy.org/) Python 3 packages.

Methods-only References

[47] Send, U., Kanzow, T., Zenk, W. & Rhein, M. Monitoring the Atlantic Meridional Overturning Circulation at 16°N. *CLIVAR Exchanges* **7**, 1–4 (2002) .

[48] Kanzow, T., Send, U. & McCartney, M. On the variability of the deep meridional transports in the tropical North Atlantic. *Deep Sea Res. Part I Oceanogr. Res. Pap.* **55**, 1601–1623 (2008). https://doi.org/10.1016/j. dsr.2008.07.011 .

[49] Johns, W. E. *et al.* Variability of Shallow and Deep Western Boundary Currents off the Bahamas during 2004–05: Results from the 26°N RAPID–MOC array. *J. Phys. Oceanogr.* **38**, 605–623 (2008). https://doi.org/10.1175/2007JPO3791.1 .

[50] McCarthy, G. D. *et al.* Measuring the Atlantic Meridional Overturning Circulation at 26°N. *Prog. Oceanog.* **130**, 91–111 (2015). https://doi.org/ 10.1016/j.pocean.2014.10.006 .

[51] Meinen, C. S. *et al.* Variability of the Deep Western Boundary Current at 26.5°N during 2004–2009. *Deep Sea Res. Part II Top. Stud. Oceanogr.* **85**, 154–168 (2013). https://doi.org/10.1016/j.dsr2.2012.07.036 .

[52] Wong, A., Keeley, R., Carval, T. & the Argo Data Management Team. Argo quality control manual for CTD and trajectory data. Tech. Rep., Ifremer (2023).

[53] Locarnini, R. A. *et al.* World Ocean Atlas 2018, volume 1: Temperature. Tech. Rep., NOAA Atlas NESDIS 81 (2018).

[54] Zweng, M. M. *et al.* World Ocean Atlas 2018, volume 2: Salinity. Tech. Rep., NOAA Atlas NESDIS 82 (2018).

[55] GEBCO Compilation Group. GBCO 2020 grid (2020).

[56] McCartney, M. S., Bennett, S. L. & Woodgate-Jones, M. E. Eastward flow through the Mid-Atlantic Ridge at 11°N and its influence on the abyss of the eastern basin. *J. Phys. Oceanogr.* **21**, 1089–1121 (1991). https://doi.org/10.1175/1520-0485(1991)021⟨1089:EFTTMA⟩2.0.CO;2 .

[57] Gupta, M. M. Numerical methods and software (David Kahaner, Cleve Moler, and Stephen Nash). *SIAM Review* **33**, 144–147 (1991). https://doi.org/10.1137/1033033 .

[58] Johns, E., Watts, R. D. & Rossby, T. H. A test of geostrophy in the Gulf Stream. *J. Geophys. Res.* **94**, 3211–3222 (1989). https://doi.org/10.1029/ JC094iC03p03211 .

[59] Danabasoglu, G. *et al.* Revisiting AMOC transport estimates from observations and models. *Geophys. Res. Lett.* **48** (2021). https://doi.org/10. 1029/2021GL093045.

[60] Send, U., Lankhorst, M. & Kanzow, T. Observation of decadal change in the Atlantic meridional overturning circulation using 10 years of continuous transport data. *Geophys. Res. Lett.* **38** (2011). https://doi.org/10. 1029/2011GL049801

[61] Akima, H. A new method of interpolation and smooth curve fitting based on local procedures. *J. ACM* **17**, 589–602 (1970). https://doi.org/10.1145/321607.321609 .

[62] Bindoff, N. L. & Mcdougall, T. J. Diagnosing climate change and ocean ventilation using hydrographic data. *J. Phys. Oceanogr.* **24**, 1137–1152 (1994). https://doi.org/10.1175/1520-0485(1994)024⟨1137:DCCAOV⟩2. 0.CO;2 .

[63] Häkkinen, S., Rhines, P. B. & Worthen, D. L. Heat content variability in the North Atlantic Ocean in ocean reanalyses. *Geophys. Res. Lett.* **42**, 2901–2909 (2015). https://doi.org/10.1002/2015GL063299 .

[64] McDougall, T. J. & Barker, P. M. Getting started with TEOS-10 and the Gibbs Seawater (GSW) oceanographic toolbox. Tech. Rep., SCOR/I- APSO WG127 (2011). URL http://www.teos-10.org/software.htm. ISBN 978-0-646-55621-5 .

[65] Jackett, D. R. & McDougall, T. J. A neutral density variable for the world's oceans. *J. Phys. Oceanogr.* **27**, 237–263 (1997). https://doi.org/10.1175/1520-0485(1997)027⟨0237:ANDVFT⟩2.0.CO;2 .

[66] Emery, W. J. & Thomson, R. E. *Data analysis methods in physical oceanography* third edn (Elsevier, Amsterdam, 2001).

[67] Biló, T. C., Straneo, F., Holte, J. & Le Bras, I. A. A. Arrival of new great salinity anomaly weakens convection in the Irminger Sea. *Geophys. Res. Lett.* **49**, 1–10 (2022). https://doi.org/10.1029/2022GL098857 .

[68] Hussain, M. & Mahmud, I. Pymannkendall: a python package for non parametric Mann Kendall family of trend tests. *J. Open Source Softw.* (2019). https://doi.org/10.5281/zenodo.3347253 .

[69] Mann, H. Nonparametric tests against trend. *Econometrica* **3** (1945). https://doi.org/10.2307/1907187 .

[70] Kendall, M. *Rank correlation methods* fourth edn (Charles Griffin, 1195 Glasgow, 1975).

[71] Yue, S. & Wang, C. The Mann-Kendall test modified by effective sample size to detect trend in serially correlated hydrological series. *Water Resour. Manag.* **18**, 201–218 (2004). https://doi.org/10.1023/B:WARM.0000043140.61082.60 .